Aalto University

OPEN ACCESS

This is an electronic reprint of the original article.
This reprint may differ from the original in pagination and typographic detail.

Hu, Yi; Cao, Meilian; Xu, Jianing; Liu, Xueying; Lu, Jiqing; Yan, Jie; Huan, Siqi; Han, Guangping; Bai, Long; Cheng, Wanli; Rojas, Orlando J.

Thermally insulating and electroactive cellular nanocellulose composite cryogels from hybrid nanofiber networks

Published in:
Chemical Engineering Journal

DOI:
10.1016/j.cej.2022.140638

Published: 01/01/2023

Document Version
Publisher's PDF, also known as Version of record

Published under the following license:
CC BY

Please cite the original version:
Hu, Y., Cao, M., Xu, J., Liu, X., Lu, J., Yan, J., Huan, S., Han, G., Bai, L., Cheng, W., & Rojas, O. J. (2023). Thermally insulating and electroactive cellular nanocellulose composite cryogels from hybrid nanofiber networks. *Chemical Engineering Journal*, *455*, Article 140638. https://doi.org/10.1016/j.cej.2022.140638

This material is protected by copyright and other intellectual property rights, and duplication or sale of all or part of any of the repository collections is not permitted, except that material may be duplicated by you for your research use or educational purposes in electronic or print form. You must obtain permission for any other use. Electronic or print copies may not be offered, whether for sale or otherwise to anyone who is not an authorised user.

Chemical Engineering Journal 455 (2023) 140638

Contents lists available at ScienceDirect

Chemical Engineering Journal

journal homepage: www.elsevier.com/locate/cej

Thermally insulating and electroactive cellular nanocellulose composite cryogels from hybrid nanofiber networks

Yi Hu [a], Meilian Cao [a], Jianing Xu [a], Xueying Liu [a], Jiqing Lu [a], Jie Yan [a], Siqi Huan [a], Guangping Han [a,*], Long Bai [a,*], Wanli Cheng [a,*], Orlando J. Rojas [b,c,*]

[a] Key Laboratory of Bio-based Material Science & Technology (Ministry of Education), Northeast Forestry University, Harbin 150040, PR China
[b] Bioproducts Institute, Department of Chemical & Biological Engineering, Department of Chemistry and Department of Wood Science, 2360 East Mall, The University of British Columbia, Vancouver, BC V6T 1Z3, Canada
[c] Department of Bioproducts and Biosystems, School of Chemical Engineering, Aalto University, FI-00076 Espoo, Finland

ARTICLE INFO

Keywords:
Cellulose nanofiber
Cryogels
Superelasticity
Thermal insulator
Electroactive materials
Sensors

ABSTRACT

Cellulose-based xerogels, cryogels and aerogels have been proposed to deliver the functions required by next-generation wearable electronics and energy materials. However, such systems often lack functionality and present limited mechanical resilience. Herein, we introduce a simple strategy to synthesize high-performance cryogels that combine cellulose and silica nanofibers that form ice-templated cellular architectures. Specifically, dual networks are produced by incorporating organic (cellulose) and inorganic (silica) nanofibers to form highly interconnected and vertically-aligned channels. Hence, ultralight structures (7.37 mg cm^{-3} in density and porosity of 99.37%) are produced with high mechanical strength, compressibility (dimensional recovery of up to 90%) and fatigue resistance (1000 loading cycles) along with low thermal conductivity (29.65 mW $m^{-1}K^{-1}$). Electrical responsiveness is supplemented by *in situ* polymerization of pyrrole, ensuing operation in a wide load range (0–18 kPa with sensitivity of 6.63 kPa^{-1} during > 1000 cycles). The obtained thermal insulating and electroactive materials are demonstrated for operation under extreme conditions (solvent and temperature). Overall, our dual network system provides a universal, multifunctional platform that can substitute state-of-the-art carbonized or carbon-based light-weight materials.

1. Introduction

Superelastic, lightweight materials that are simultaneously fatigue resistant fit ideally the needs of wearable electronics [1,2], flexible sensors [3,4], and portable devices [5,6], among others. Particularly, development of electroactive sensors has become an active research area owing to their wide use, for instance, in health diagnosis and physiological monitoring [7,8]. Moreover, the next-generation sensors need to perform in a wide range of environments and, for such purpose, cryogels exhibiting compressibility, conductivity, and thermal insulation properties are ideal, provided they are strong and sustain extreme conditions [9,10]. Considering electrical conductivity, cryogels are often produced from expensive, synthetic building blocks, such as carbon nanofibers [11] and nanotubes [12], graphene oxide [13] and MXene [14], all of which are associated with costly and energy-intensive processing. In addition, they exhibit uncontrollable volume shrinkage and resistivity, and are associated with negative carbon footprint [15]. Therefore, there is a pressing need for sustainable, non-carbonaceous, elastic and cost-effective cryogels.

Naturally-derived materials are ideal alternatives for synthesizing sustainable cryogels. Moreover, organic–inorganic hybridization is effective to improve the elasticity of biobased cryogels while retaining their lightweight [16]. For instance, hybrid cryogels composed of entangled dual fibers, cellulose nanofibrils (CNF) and silica fibers, showed improved flexibility and formability [17,18]. However, the typical uncontrollable, disorganized microstructures prevalent in hybrid cryogels undermine the potential benefits of the inorganic phase. To overcome this issue, structural design can be considered, for instance, following the example of living organisms [19], including wood and its highly aligned cellular structure formed by cellulose microfibers [20]. The latter are tightly entangled in macrofibers embedded in a matrix (containing lignin and hemicellulose) that maximize strength [21,22].

* Corresponding authors at: Bioproducts Institute, Department of Chemical & Biological Engineering, Department of Chemistry and Department of Wood Science, 2360 East Mall, The University of British Columbia, Vancouver, BC V6T 1Z3, Canada (O.J. Rojas).
E-mail addresses: guangping.han@nefu.edu.cn (G. Han), long.bai@nefu.edu.cn (L. Bai), nefucwl@nefu.edu.cn (W. Cheng), orlando.rojas@ubc.ca (O.J. Rojas).

https://doi.org/10.1016/j.cej.2022.140638
Received 7 September 2022; Received in revised form 7 November 2022; Accepted 24 November 2022
Available online 29 November 2022
1385-8947/© 2022 The Author(s). Published by Elsevier B.V. This is an open access article under the CC BY license (http://creativecommons.org/licenses/by/4.0/).

By using chemical treatment, it is possible to produce compressible and elastic sponge-like materials from wood [23–25]. Although such wood-derived sponge retains the unique hierarchical nanostructure and high specific surface area of the precursor, the synthesis involves chemically-intensive processes. Hence, an alternative route to achieve the desired properties involves cryogels that emulate the hierarchical characteristics encoded in natural wood.

Inspired by wood biomimicry, we develop a hybridization strategy to produce cryogels with an ordered, cellular-like structure composed of cellulose nanofibrils (CNF, TEMPO-oxidized) and a mineral phase (silica). In this design, CNF acts as the skeleton of the cryogel, which benefits from unique porous and structural templating [26]. Meanwhile, electrospun silica nanofibers are embedded in the scaffold and improve the microstructure of the cryogel by connecting with CNF, achieving an excellent balance between elasticity and fatigue resistance (> 1000 loading cycles, maintaining 82.99% of maximum stress), as well as thermal insulation (29.65 mW $m^{-1}K^{-1}$ heat conductivity). The hybrid and superelastic cryogels are further modified to develop electrical conductivity through *in situ* polymerization of pyrrole, forming polypyrrole (PPy) that crosses the lumen of the cells. When acting as an electroactive sensor, the cryogel shows a high sensitivity (up to 6.63 kPa^{-1}) under a broad range of pressure (0–18 kPa) and an excellent durability (1000 cycles). Hence, flexibility and electroactivity are achieved with the hybrid, non-carbonaceous cryogels, ideally suited for high-performance, multifunctional devices.

2. Experimental section

2.1. Materials and chemicals

Cellulose nanofibrils with a length and diameter of approximately 1–2 μm and 10–20 nm, respectively, were purchased as aqueous suspension from Tianjin Woodelf biotechnology Co. ltd (Tianjin, China). The nanofibrils were produced from bleached kraft hardwood pulp using TEMPO-mediated oxidation (carboxylate content of *ca.* 1.4 mmol/g). For simplicity, we refer to the oxidized cellulose nanofibrils as CNF. Tetraethyl orthosilicate (TEOS), polyvinyl alcohol (PVA, 1788), methyltrimethoxysilane (MTMS), phosphoric acid, and hydrochloric acid were obtained from Aladdin (Shanghai, China). The hydrolyzed MTMS sol was prepared by mixing 0.5 g of MTMS solution, 0.5 g of hydrochloric acid solution (0.1 M), and 4.5 g of deionized (DI) water, following with continuously stirring for 2 h to fully hydrolyze MTMS. All reagents were analytical grade and used as received without any further purification.

2.2. Sol-gel electrospinning of SiO_2

An aqueous solution of PVA (10 wt%) was prepared by stirring 2 g PVA in 18 g water at 85 °C for 2 h. Silica precursor sol solution was prepared by mixing TEOS:H_3PO_4:H_2O in 1:0.01:11 molar ratio and stirred at room temperature for 8 h to obtain silica sol solution. Subsequently, the silica precursor sol solution was slowly added to 10 wt% PVA solution at a mass ratio of 1:1 and stirred for 4 h to obtain a homogeneous spinning solution. The solution was loaded into a 5-ml syringe and pumped at a constant rate (1 ml h^{-1}) under an applied electrospinning high voltage of 20 kV. The ambient temperature and relative humidity were 25 ± 5 °C and 45 ± 5%, respectively. To obtain the silica nanofibers, the PVA/TEOS hybrid membranes were calcined at 800 °C in air for 2 h at a heating rate of 5 °C min^{-1}. For simplicity, these fibers are referred to as SiO_2 or silica nanofibers.

2.3. Preparation of CNF/SiO_2 cryogels

Briefly, 23 g CNF aqueous suspension (1.3 wt%) and 0.2 g SiO_2 nanofiber membrane were dispersed in deionized water, wherein the mixture was homogenized at high speed (19000 rpm, SCI-160 homogenizer) for 20 min to obtain a homogeneous dispersion with a total solid content of 0.5 wt%. Then, hydrolyzed MTMS sol (crosslinking agent) was slowly added into the dispersion, and the mixture was stirred for 2 h to ensure full reaction. The mass ratio of MTMS:CNF:SiO_2 was 5:3:2. Subsequently, the obtained dispersion was frozen in a specially-designed mold attached to a copper base cooled with liquid nitrogen, following by drying the sample for at least 36 h in the freeze-dryer (-50 °C and 4 Pa) to obtain cryogel. According to the mass ratio of CNF-to-SiO_2, a series of cryogels were obtained, referred to as CNF/SiO_2-0 (5/0), CNF/SiO_2-1 (4/1), CNF/SiO_2-2 (3/2) and CNF/SiO_2-3 (2/3).

2.4. Preparation of PPy@CNF/SiO_2 cryogels

The PPy@CNF/SiO_2 cryogels were fabricated by *in situ* polymerization of pyrrole. Briefly, the as-prepared CNF/SiO_2 cryogels were fully immersed into ethanol and exchanged with 0.5 M HCl to tailor their wettability. Based on preliminary experiments and considering the level of electrical conductivity and performance of the cryogels, a 0.1 M pyrrole solution was used to form PPy. Briefly, pyrrole solution was prepared by dissolving the given amount of pyrrole in 0.5 M HCl with continuous stirring at room temperature. The pretreated CNF/SiO_2 cryogels were then added to the above solution and left at rest for 2 h to allow pyrrole to completely penetrate into the interior of the cryogels. Following, the as-prepared cryogels were placed in a $FeCl_3$ solution (0.2 M $FeCl_3{\cdot}6H_2O$ dissolved in 0.5 M HCl) with an ice-water bath at 0 °C for 6 h. After reaction, and to remove residual pyrrole and $FeCl_3$, the samples were repeatedly washed with ethanol and deionized water. Finally, the PPy@CNF/SiO_2 cryogels were frozen in a refrigerator at -18 °C for at least 24 h, followed by drying in a freeze-dryer (-50 °C and 4 Pa) for at least 48 h.

2.5. Characterization

The morphology of the cryogels was followed by scanning electron microscopy (SEM, JEM-7500F, JEOL, Japan) and elemental mapping was recorded using EDS spectroscopy attached to the SEM. The surface functional groups were identified by Fourier Transform Infrared Spectroscopy (FTIR) using Nicolet iN10 Spectrometer (Thermo Fisher Scientific Inc., USA). The surface chemical composition was confirmed using X-ray photoelectron spectrometer (K-Alpha, Thermo Fisher Scientific Inc., USA). Cryogel samples with size of 20 × 20 × 20 mm^3 were prepared for compression tests: compression, elasticity, and fatigue resistance were recorded on a universal testing machine (Suns, UTM2503, China) with a 100-N load cell and compression speed of 10 mm/min. The thermal stability of the cryogels was evaluated by thermogravimetric (TG) analysis using a thermal analyzer (DSC/DTA-TG, STA449 F3, Netzsch, Germany) by heating from room temperature to 800 °C (heating rate of 10 °C min^{-1}) under nitrogen atmosphere. Thermal conductivity was measured by a Hot Disk TPS 2500 S instrument (Hot Disk AB, Sweden), and thermographic images were taken with an infrared thermal camera (Testo 869, Testo AG, Germany).

The PPy@CNF/SiO_2 sensor was fabricated by assembling a conductive cryogel between two polyethylene terephthalate (PET) supports, adhered with two copper sheets. The compression-strain profiles of the PPy@CNF/SiO_2 sensor were recorded by connecting the universal testing machine (Suns, UTM2503) with an electrochemical workstation (CHI 660E, applying a voltage of 1 V). Signal detection of human motions was carried out with the help of a volunteer who was installed with the PPy@CNF/SiO_2 sensor. The gauge factor (GF) for sensitivity of strain sensors was calculated according to the following formula:

$$GF = (\Delta R/R_0)/\varepsilon$$

where R_0 is the initial resistance of the PPy@CNF/SiO_2 sensor (without pressure), ΔR is the relative change in resistance, and ε is the applied stain. The sensitivity (S, kPa^{-1}) of the sensors was calculated according to the following formula:

$S = \delta(\Delta I/I_0)/\delta P$

where I_0 is the initial current of the PPy@CNF/SiO_2 sensor (without pressure), ΔI is the relative change in current, and δP is the change of the applied pressure.

3. Results and discussion

3.1. CNF/SiO_2 cryogels

Elastic, conductive nanofiber-based cryogels are designed considering a number of features. Fist, flexible nanofibers are assembled into a robust 3D framework, leading to a cellular-like, ordered, open-pore structure. Secondly, cryogels are formed to enable mechanically strong but deformable light-weight materials. Finally, electrical conductivity is optionally added by *in situ* synthesis of polypyrrole (PPy). In this design, the ordered internal microstructure is achieved by directional freezing, incorporating CNF and electrospun silica (SiO_2) nanofibers that are tightly entangled. Hydrolyzed methyltrimethoxysilane (MTMS) is added to further reinforce the connections between CNF and the SiO_2 nanofibers by reaction with CNF's surface hydroxyl groups. The obtained system can preserves the ordered microstructure achieved by directional freezing but enhances its mechanical strength, compressibility and flexibility.

Our three-step synthesis of CNF/SiO_2 cryogels firstly involved SiO_2 nanofibrous membranes prepared by sol–gel electrospinning [27], where the fiber (diameter of 357 nm) formed a highly flexible structure (Fig. 1 and S1). For this purpose, the CNF aqueous suspension was combined with the SiO_2 nanofiber membranes and homogenized to reduce the length of the SiO_2 nanofibers to about 84 μm, which was still much longer than that of CNF (Figure S2). This enabled entanglement with CNF and formation of a skeleton with adjusted CNF/SiO_2 nanofiber ratio in the presence of MTMS that was used as a binder. The nanofiber dispersion was directionally frozen with liquid nitrogen, and then freeze-dried to generate MTMS-bound CNF/SiO_2 cryogels. Benefitting from ice crystal nucleation and phase separation between CNF/SiO_2 nanofibers and ice crystals, interconnected, ordered, cellular-like structures were formed within the network, composed of a dual nanofiber system. According to the relative mass ratio of CNF/SiO_2 at 5/0, 4/1, 3/2 and 2/3, the cryogels are referred to as CNF/SiO_2-0, CNF/SiO_2-1, CNF/SiO_2-2 and CNF/SiO_2-3, respectively. As a last optional step, PPy was polymerized *in situ* within the CNF/SiO_2 cryogels using the respective monomer (PPy@CNF/SiO_2).

3.2. Morphology and material characterization

Hydrogen bonding of surface hydroxyl groups of CNF enabled self-supporting cryogels and prevented volume shrinkage of the CNF/SiO_2 system during freeze-drying [28]. The flexible, high-aspect-ratio SiO_2 nanofibers strengthened the CNF scaffold, improving the mechanical strength and structural stability. Upon reaction, hydrolyzed MTMS molecules reacted with hydroxyl groups of CNF and bound SiO_2 nanofibers, preventing slippage between the dual nanofibrous network and improving its surface hydrophobicity (Figure S3) [29].

The as-prepared cryogels revealed a porous, ordered cellular-like structure consisting of open-cell walls and interconnected hybrid nanofibers (SEM images, Fig. 2a-2e). The formation mechanism leading to ordered cellular structures was mainly produced by directional ice templating following the three-phase change of water under a suitable temperature gradient during freezing and freeze-drying [30]. We note the microstructure of neat CNF cryogels, Fig. 2a, which exhibited a low-elasticity, disordered lamellar microporous structure and a random

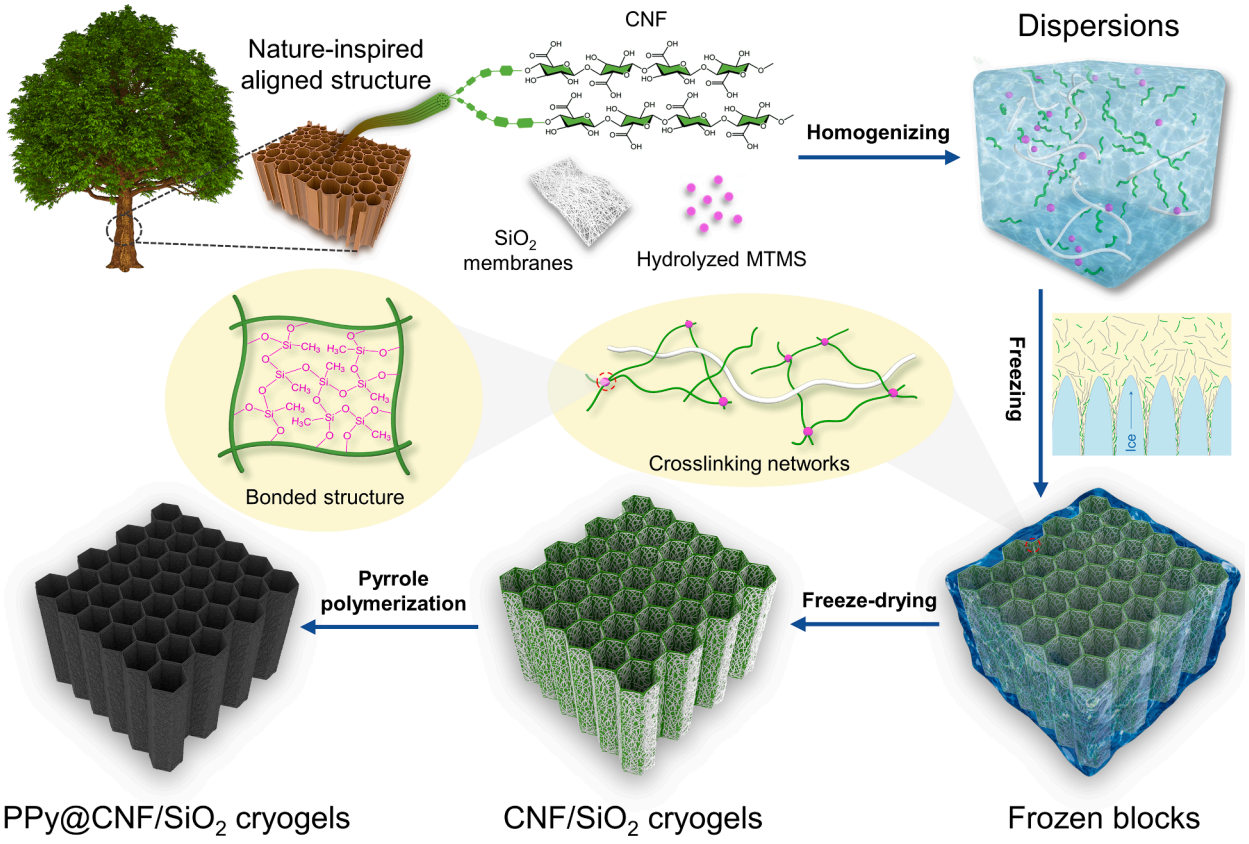

Fig. 1. Schematic illustration (not to scale) of synthesis of CNF/SiO_2 cryogel. Homogenized CNF/SiO_2 nanofibers and MTMS were first prepared through high-speed homogenization, and then the dispersion was directionally freeze-dried into CNF/SiO_2 cryogels. The resultant CNF/SiO_2 cryogel was loaded with PPy after *in situ* polymerization of pyrrole, obtaining an electrically conductive cryogel (PPy@CNF/SiO_2).

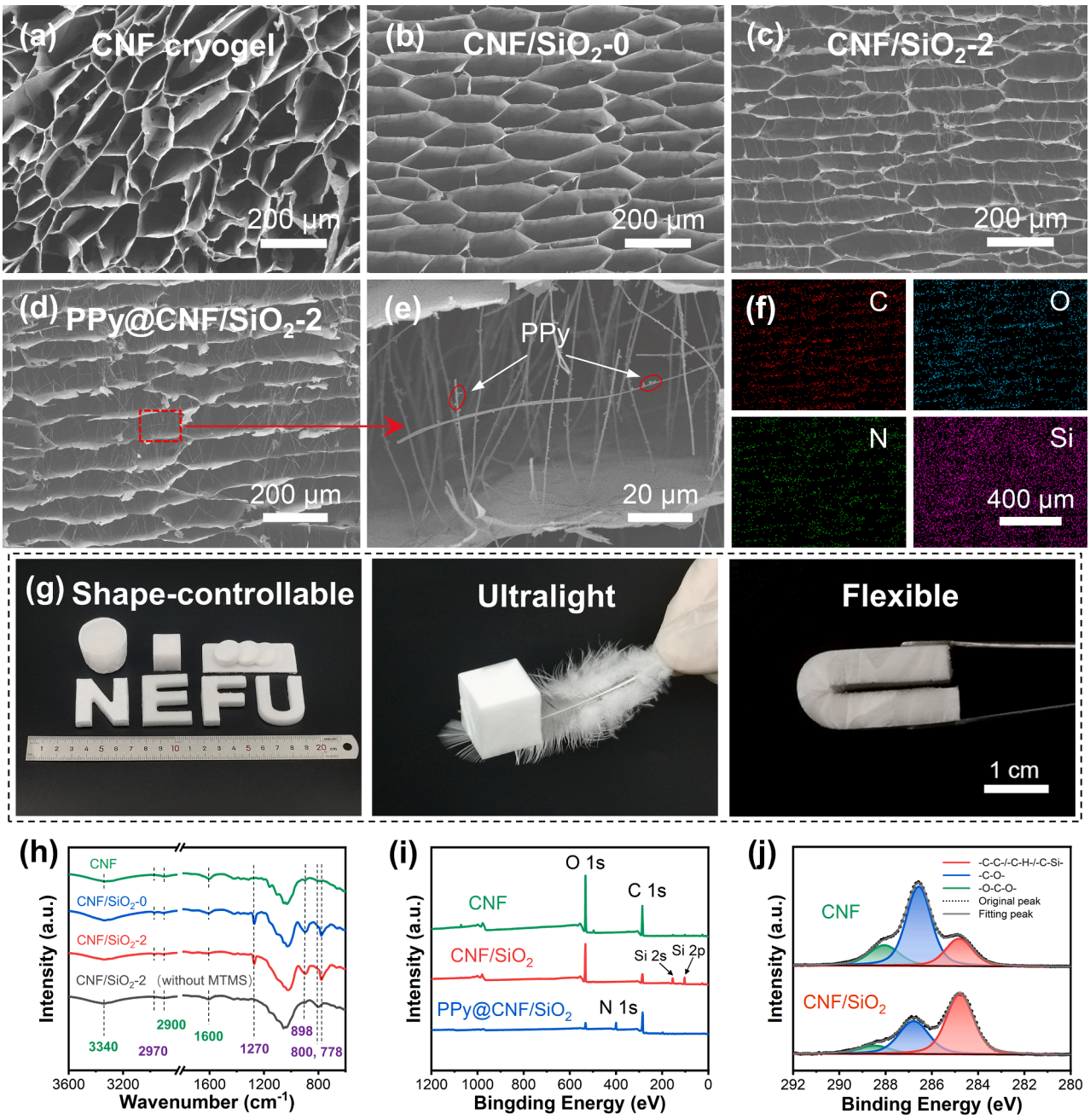

Fig. 2. Morphology and material characterization of CNF/SiO_2 cryogels. SEM images of (a) pure CNF cryogel, (b) CNF/SiO_2-0, (c) CNF/SiO_2-2, (d) and (e) PPy@CNF/SiO_2-2 showing nanofibers and pore walls coated with PPy. The red circles in (e) highlight aggregated PPy protruding on the SiO_2 nanofibers. (f) EDS elemental (C, O, N, and Si) mapping images of PPy@CNF/SiO_2-2. (g) Photographs displaying the shape-controllable, ultralight and flexible CNF/SiO_2-2 cryogels. (h) FTIR and (i) wide XPS spectra of as-prepared cryogels. (j) C 1 s spectra of pure CNF and CNF/SiO_2-2 cryogels.

three-dimensional assembly that included thin sheets and nanofilaments. The structure formed by CNF resulted from the entanglement of the fibrils during ice growth, resulting in a continuous but disordered system. Comparatively, MTMS-crosslinked CNF cryogels (CNF/SiO_2-0, mass ratio of CNF/SiO_2 = 5:0) presented a regular and uniform structure (Fig. 2b). The addition of MTMS not only facilitated the formation of more uniform ice crystals, but also reduced CNF aggregation.

The length of the cell system gradually increased with the loading of SiO_2 nanofibers, forming a parallel "layer-strut" with inter-linked fibers (*ca.* 50 μm) between the thin cell walls. The results indicated that SiO_2 nanofibers facilitated parallel alignment of CNF (Fig. 2c and Figure S4), which was attributed to the strength of the long electrospun nanofibers during freezing. The CNF/SiO_2-2 (mass ratio of CNF/SiO_2 = 3/2) indicated SiO_2 nanofibers connected and entangled with the cellulose counterparts, embedded within the CNF skeleton, which mechanically reinforced the system and enabled elasticity *via* efficient energy dissipation. The strong interaction between the nanofiber components in the hybrid system played a key role in creating ordered architectures. Meanwhile, directional ice templating led to the formation of an anisotropic structure. By freezing the nanofiber dispersion, the CNF and SiO_2 nanofibers were displaced and concentrated in the interstitial space between the growing ice crystals and produced a tracheid-like texture (Figure S5) [31].

After *in situ* polymerization of pyrrole, Fig. 2d and 2e, the cryogel morphology was largely retained, and PPy particles were observed to be randomly distributed on the surface of the nanofibers and pore walls,

crossing the lumen of the cells and forming a continuous nano-sheath structure [32]. The latter observation was confirmed by energy-dispersive X-ray spectroscopy (EDS) mapping, wherein C and O atoms were uniformly distributed along the walls of the cryogels (Fig. 2f), revealing that CNF was the main component. Due to MTMS crosslinking and the presence of SiO_2 nanofibers, Si was randomly dispersed throughout the space. Meanwhile, the N signal, characteristic of PPy, was evenly distributed within the cells, indicating that the conductive polymer formed uniformly on the surface and across the pore walls [33].

The CNF/SiO_2 cryogels showed excellent shape flexibility and low density (Fig. 2g). For instance, the cryogels easily shaped into 3D objects. The CNF/SiO_2 cryogels were ultralight (≈7.37 mg cm^3, Table S1) and were supported by a feather, with no bending deformation. In addition, the as-prepared cryogels were easily folded in half, with no rupture, and rapidly recovered the initial state after unloading.

We used FTIR and XPS to investigate the chemical structure and interactions between CNF and SiO_2 nanofibers in the CNF/SiO_2 cryogels (Fig. 2h to 2j). FTIR spectra of neat CNF cryogels showed peaks at 3340, 2900 and 1600 cm^{-1}, corresponding to the stretching vibration of –OH, CH_2 and C═O (sodium carboxylate groups were introduced during TEMPO oxidation [34]) (Fig. 2h). After modification with MTMS and SiO_2, additional FTIR peaks at 2970, 1270, and 898 cm^{-1} and between 800 and 778 cm^{-1} appeared, assigned to the ν(C—H) of the methyl groups δ(Si-CH_3), ν(Si-OH) of hydrogen bonds with cellulose hydroxyl groups, and ν(Si-O-Si) and/or ν(Si-C), respectively [28]. These results indicated the formation of covalent bonds between CNF and hydrolyzed MTMS.

Wide XPS elemental spectra showed C and O as the main elements in the CNF cryogel, while the other composite cryogels included C, O, and Si (Fig. 2i). For PPy@CNF/SiO_2-2, the characteristic N elemental peak of PPy was observed. The C 1 s spectra revealed the characteristic C peaks at 284.8, 286.8, and 288.3 eV (Fig. 2j), assigned to sp^2 C, -C—O-, and -O—C—O-, respectively [35]. After crosslinking, the peak at 284.8 eV increased markedly, from 22% (CNF) to 58% (CNF/SiO_2-2), implying the formation of C-Si binds mediated by MTMS [36]. Simultaneously, the XPS spectra of PPy@CNF/SiO_2 confirmed that a stable PPy shell layer was produced on the inner surface of the cryogels (Figure S6 and discussion in Supporting Information).

3.3. Mechanical and shape adaptability

To explore the mechanical properties of CNF/SiO_2 cryogels, we compared the compressive stress–strain profiles of different samples using a 50% strain loading. As shown in Fig. 3a, both yield stress and elasticity increased with SiO_2 nanofiber loadings, up to an optimal mass ratio of CNF/SiO_2 (3/2), showing only 1.49% plastic deformation and relatively high compressive strength (4.92 kPa, strain = 50%). Fig. 3b presents the compressive stress–strain curves of CNF/SiO_2-2

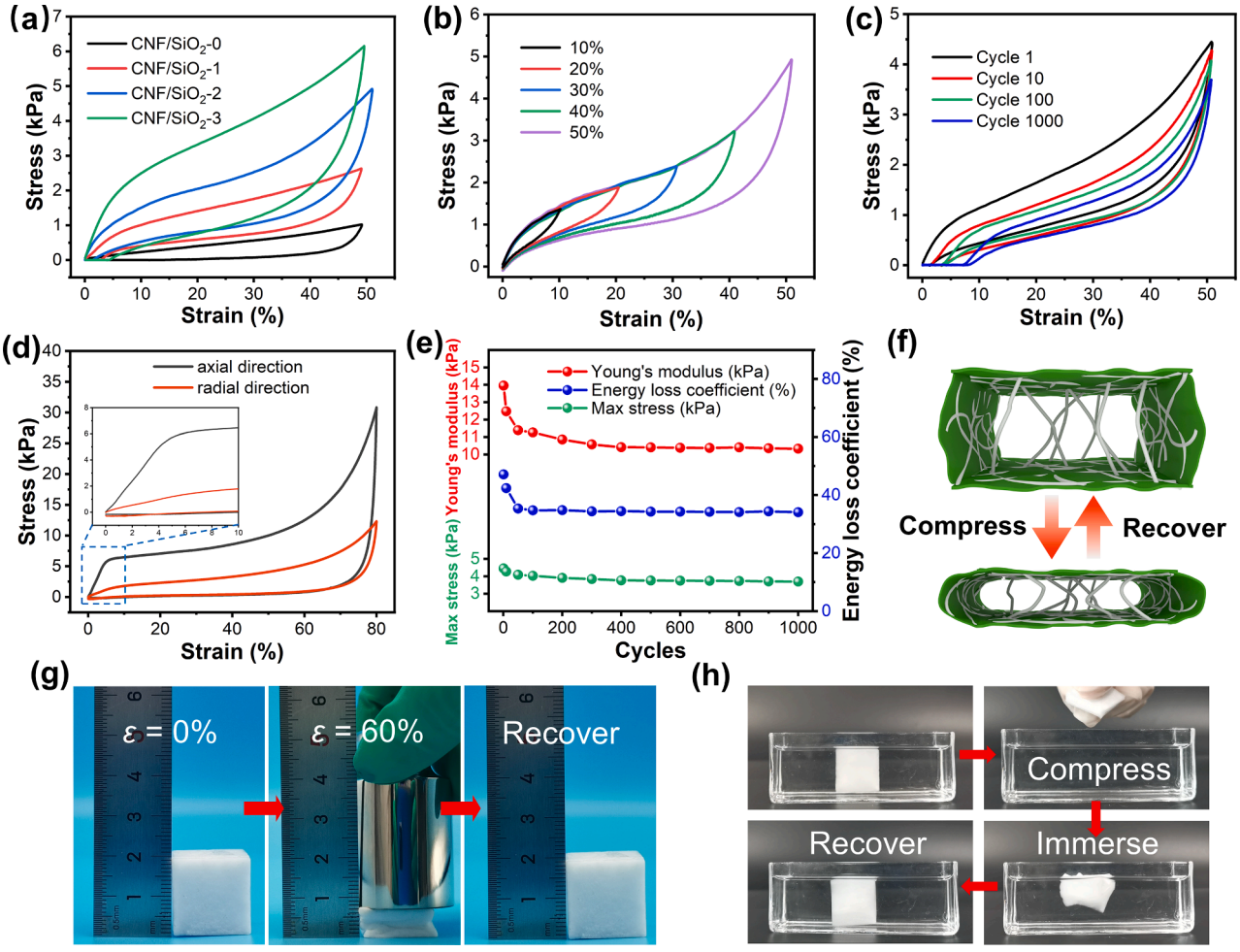

Fig. 3. Mechanical strength and shape-recovery of CNF/SiO_2 cryogels. (a) Stress–strain profiles of samples subjected to 50% strain. (b) Stress–strain curves at given strains. (c) Fatigue resistance at 50% strain for 1000 cycles. (d) Stress–strain curves along different directions at 80% strain. (e) Young's modulus, energy loss coefficient and max stress at 50% strain following 1000 loading/unloading cycles. (f) Schematic illustration (not to scale) of the compression and recovery of cell structure. Photographs illustrating (g) instantaneous shape recovery of cryogels CNF/SiO_2-2 initially infused with ethanol following loading and unloading and (h) compressive deformation and full recovery in ethanol.

corresponding to the loading/unloading cycles at a set series of strain (10 to 50%), which indicates that the maximum compressive strain gradually increased from 10% to 50%. The CNF/SiO_2-2 system recovered its initial height after unloading. Recovery after multiple cycles of long-term compression is critical in most practical applications. The CNF/SiO_2-2 cryogel recovered its original shape and size after unloading, even after 90% deformation (strain) in the radial direction (Video S1). The CNF/SiO_2-2 was further subjected to fatigue hysteresis tests following 1000 loading–unloading compressive cycles at 50% strain (Fig. 3c), showing that the cryogel largely recovered the initial shape. Only a slight plastic deformation (3.57% at the 100th cycle and 7.14% at the 1000th cycle) were noted. The observations highlight an excellent fatigue resistance. The anisotropic cryogel exhibited excellent elasticity and compression resistance in both directions (Fig. 3d), which is a typical characteristic of foam-like structures.

We note a three-stage deformation regime that included a linear elastic region (< 10% strain), a plateau stage at intermediate strain (from 10% to 60%), and a densification stage with the stress increasing sharply at a high strain value (over 60%). Surprisingly, no significant reduction of the Young's modulus, energy loss coefficient, and maximum stress of CNF/SiO_2-2 was observed after 1000 cycles. Over 70% of the initial modulus and 80% of the maximum stress were maintained, demonstrating that the CNF/SiO_2-2 cryogel had an outstanding mechanical performance and structural stability (Fig. 3e). Upon loading and unloading, the flexibility of CNF and SiO_2 nanofibers allowed the tracheid-like structure to freely fold and recover, effectively dissipating stress and resulting in excellent elasticity (Fig. 3f). Moreover, the CNF/SiO_2-2 cryogel was elastic when compressed under a heavy weight (Fig. 3g) and under immersion in liquid nitrogen (-196 °C) (Video S2), indicating superelastic and adaptability under extreme low temperature.

The shape recovery features of the CNF/SiO_2-2 cryogel was further demonstrated with tests following an initial deformation and holding during a given time, indicating a full shape recovery [37]. We note that MTMS-crosslinked cryogels, with their reduced free surface hydroxyl groups (from CNF), enabled a relatively high water resistance. On the other hand, an ethanol-impregnated CNF/SiO_2-2 cryogel was compressed into a thin sheet and, upon unloading, the channels expanded back to their original shape (Fig. 3h and Video S3). The continuous cellular structure quickly swelled, following ethanol impregnation by capillarity. The strong hydrogen bonding and stable structure prevented internal cellular channels from collapsing during compression [38]. In sum, excellent mechanical strength and shape-recovery properties were confirmed for CNF/SiO_2-2 cryogel.

Taking advantage of the dual network pore structure of CNF/SiO_2 cryogels, they can be considered as a matrix for electroactive materials. As shown in Figure S7, after uniform incorporation of PPy, the PPy@CNF/SiO_2 cryogels exhibited better compressibility and fatigue resistance compared to respective unmodified CNF/SiO_2-2. This observation can be attributed to the high number density of PPy crosslinking sites. Notably, compared with the unmodified cryogel, the PPy@CNF/SiO_2 sample demonstrated a remarkably higher compressive strength

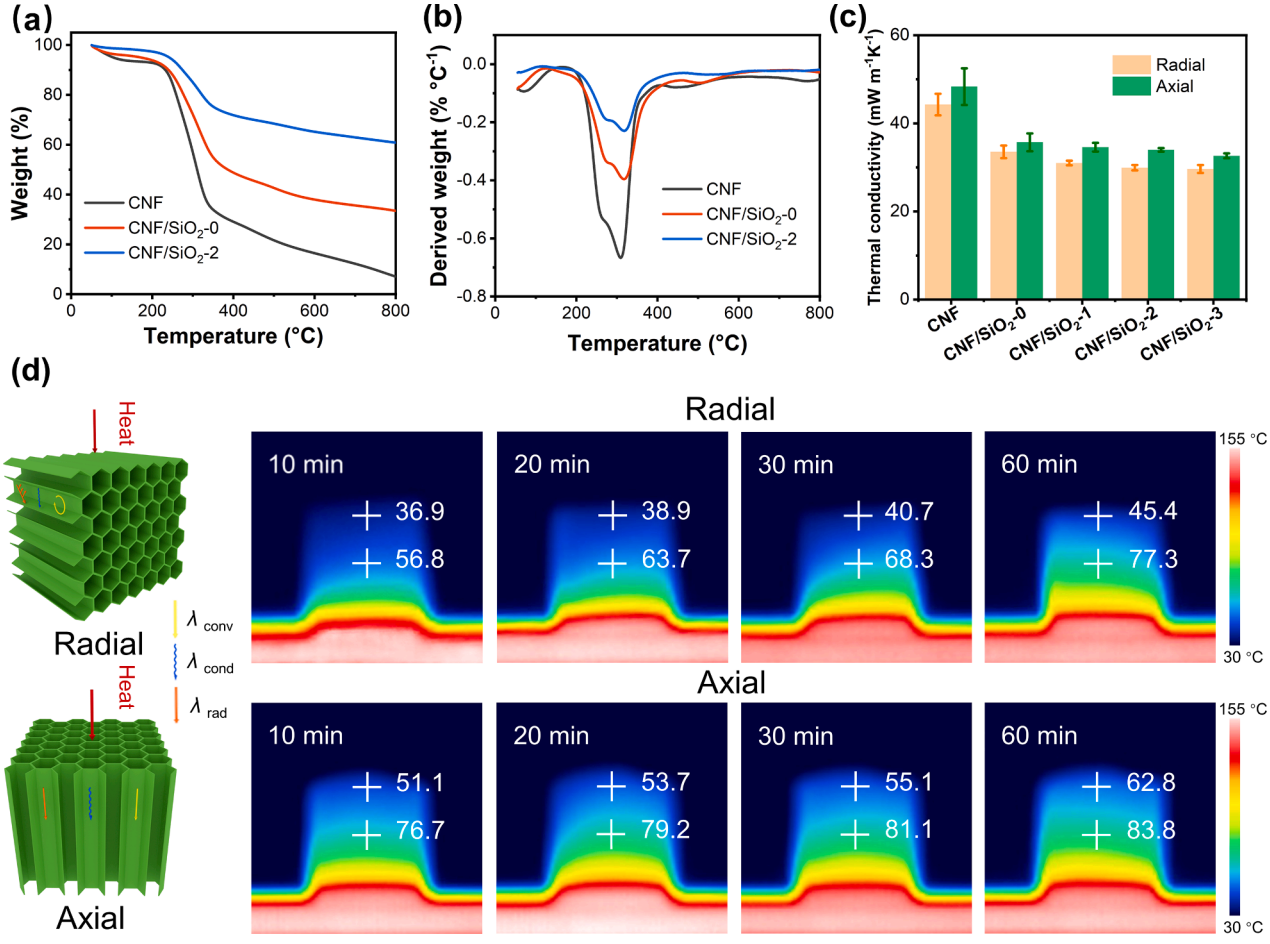

Fig. 4. Thermal stability and anisotropic thermal insulation performance of CNF/SiO_2 cryogels. (a) TG and (b) DTG curves of CNF, CNF/SiO_2-0, and CNF/SiO_2-2. (c) Average thermal conductivity of CNF and CNF/SiO_2 cryogels in the radial and axial directions. (d) Schematic illustration (not to scale) of the heat transfer mechanism of CNF/SiO_2 cryogels in the radial (upper) and axial (bottom) directions and infrared images of CNF/SiO_2 cryogel placed on a hot plate heated to 150 ℃ for 10, 20, 30 and 60 min.

(6.52 kPa, strain = 50%), lower plastic deformation (2.83% at the 1000th cycle), and higher Young's modulus, suggesting that the PPy-loaded conductive cryogels presented excellent structural stability and mechanical strength.

3.4. Thermal insulation

Thermogravimetric (TG) analyses were performed to explore the thermal stability of CNF and CNF/SiO_2 cryogels (Fig. 4a), showing that the addition of MTMS and SiO_2 nanofibers decreased the weight loss rate, which is attributed to the high thermal stability of SiO_2 nanofibers. The presence of crosslinked silica network also blocked the volatile composition and heat generated by cellulose pyrolysis (see analysis in the Supporting Information).[33] This result was supported by the DTG peaks of CNF/SiO_2-0 (Fig. 4b), which showed a shift to higher temperatures (from 309 to 318 °C) and a significantly lower weight loss (residual weight increased from 7.07% to 33.5% after crosslinking with MTMS). In sum, the addition of MTMS and SiO_2 nanofibers improved the thermal stability of the CNF-based cryogels.

Benefitting from the high thermal stability, we studied the insulation properties of the CNF/SiO_2 cryogels. The thermal conductivity of the neat CNF cryogel measured in the radial and axial directions were 44.3 and 46.3 mW m^{-1} K^{-1}, respectively (Fig. 4c). With increased addition of SiO_2 nanofibers, the thermal conductivity of the CNF/SiO_2 cryogels gradually decreased, given their more regular and uniform microstructure. The CNF/SiO_2 cryogels showed the lowest radial and axial thermal conductivity (29.7 and 34.5 mW $m^{-1}K^{-1}$, respectively) at a mass ratio of 2/3. The measured thermal conductivity and density were lower compared to other reported cryogels (Figure S8 and Table S2). As illustrated in Fig. 4d, the thermal conductivity of highly porous materials in air results, in theory, from the contribution of conduction, convection, and radiation (with the latter being ignored at ambient temperature) [39]. When the thermal energy is propagated along the radial direction, the parallel "layer-strut" structure of CNF/SiO_2 cryogels was expected to effectively weaken the solid heat conduction and restrict thermal convection *via* multiple refraction and scattering at solid-air interfaces. Hence, a significant reduction of total thermal conductivity occurred (enhanced thermal insulation).

The anisotropic cryogels, as expected, displayed direction-dependent thermal conductivity. In the axial direction, heat was transferred through the cavity of the cell structure, resulting in higher thermal conductivity compared to that in the radial direction [40]. Hence, thermal dissipation was favored along the axial direction, while the insulation performance was more significant in the radial direction. The discussed anisotropy was confirmed by irradiating a cryogel with a red-light beam (Figure S9), wherein the light passed through when directed along the axial direction but was blocked along the radial direction. The anisotropic thermal insulation performance of CNF/SiO_2 cryogels along the radial and axial directions was further demonstrated by infrared imaging when the system was placed on a hot plate kept at 150 °C. Once the cryogel reached a stable temperature, the heat transfer through the cryogel on the side of the samples (20 × 20 × 20 mm^3) was monitored (see temperature *versus* height profile in Figure S10). The temperature of the samples measured at a given height, upon placing a cryogel in the axial direction on a hot place, was significantly higher than that measured in the radial direction, indicating a much better thermal insulation performance in the latter case. Heat transfer in the axial direction was effective in the first 10 min, while the surface temperature was maintained at 45.4 °C in the radial direction (for a hot plate temperature of 150 °C), only slightly higher than the initial temperature, indicating that heat transfer was effectively blocked by the cryogel, which displayed a long-lasting high thermal stability. Overall, the results show that structural and nanoscale features of the designed cryogels enabled insulation and excellent properties from the combination of cellulose and other nanosized fibrous materials [41].

3.5. Pressure sensitivity of PPy@CNF/SiO_2

The structural stability and fatigue resistance of the CNF/SiO_2 cryogel make them a promising candidate for electroactive sensing. As such, three-dimensional conductive networks were formed in the CNF/SiO_2 cryogel with the addition of the conductive polymer (PPy), forming PPy@CNF/SiO_2. The electroactive and sensing performance were tested in a device comprising PPy@CNF/SiO_2 sandwiched between two polyethylene terephthalate (PET) films adhered with copper sheets (Figure S11). Fig. 5a reveals the real-time current response of PPy@CNF/SiO_2 during 5 cycles under given compression strain, from 20% to 80%. As expected, the current increased rapidly and significantly under compression, indicating a highly sensitive conductivity and fast response capability under compressive strain. Furthermore, the real-time *I-V* curves at given loads demonstrated that the assembled conductive cryogels were sensitive in a wide range of pressures (Fig. 5b). Under an increased external pressure, the pores surrounded by a dual nanofiber network reached close contact; hence, the distance between the PPy@CNF/SiO_2 conductive layers decreased, leading to lower contact electrical resistivity and thus increasing the current. In addition, characteristics of the linear *I-V* curves suggested a stable resistance of the PPy@CNF/SiO_2 sensor under different pressures. Furthermore, the electrical current was maintained almost at the same level after 1000 cycles at 50% strain (Fig. 5c), demonstrating PPy@CNF/SiO_2 cryogels with an excellent current stability, given the high compressibility and superelastic networks.

We further evaluated the sensitivity of the cryogel when tested as strain sensor using the gauge factor (GF) [42]. PPy@CNF/SiO_2 showed a high GF, 9.38 (strain < 4%) (Fig. 5d), demonstrating a steady linear and sensitive relationship between current output and strain. Moreover, the sensitivity (S, kPa^{-1}) of the PPy@CNF/SiO_2 sensors was used to evaluate their ability to monitor deformations [8]. A linear relationship between $\Delta I/I_0$ and pressure change is critical for a sensor to accurately report output signals. The sensitive current response to different pressures is shown in Fig. 5e. The linear S of the PPy@CNF/SiO_2 was 6.63 (R^2 = 0.9986) for a pressure range between 0 and 18.21 kPa, demonstrating a linear relationship between current output signal and applied pressure in a wide working range. The linear S was not only superior to other cellulose-based cryogels, but higher than those reported for carbon-based cryogels (Fig. 5f and Table S3) [43–53]. The excellent S of PPy@CNF/SiO_2 is attributed to the highly compressible, elastic, ordered tracheid-like architecture and the uniform PPy coverage.

The cryogel-based sensors showed underwater electrical conductivity, involving three stages of current change: stabilization, loading compression and underwater self-recovery, given the shape-memory property of the cryogels (Fig. 5g). This current response was stable and durable, showing full recovery of the initial value without observable shift after removal of the pressure. More importantly, given the excellent physical properties of the CNF/SiO_2 cryogel, PPy@CNF/SiO_2 exhibited a relatively stable cyclic stability at low (liquid nitrogen, Figure S12) and high (50, 100, and 150 °C, Fig. 5h) temperatures. The change of current under different applied pressures was further demonstrated by connecting the cryogel sensor with a light-emitting diode (LED) circuit (Fig. 5i). The luminance of green LED varied with the loading pressures (it became brighter at an increased external force, from 0 to 12.4 kPa), reflecting an increase in current (reduced resistance) under load.

Considering remarkable mechanical performance, deformability, excellent sensitivity, and strain/pressure detection capability of PPy@CNF/SiO_2, the cryogels were tested as a wearable device. They reliably captured the bending movement when attached to a finger, as registered by the current signals measured at given bending angles (Fig. 5j). The $\Delta I/I_0$ signals intensified with the increase in bending angle and stayed almost unchanged when keeping the finger at a given bending angle, demonstrating real-time stability and responsiveness. The time-dependent changes in the electrical current were demonstrated

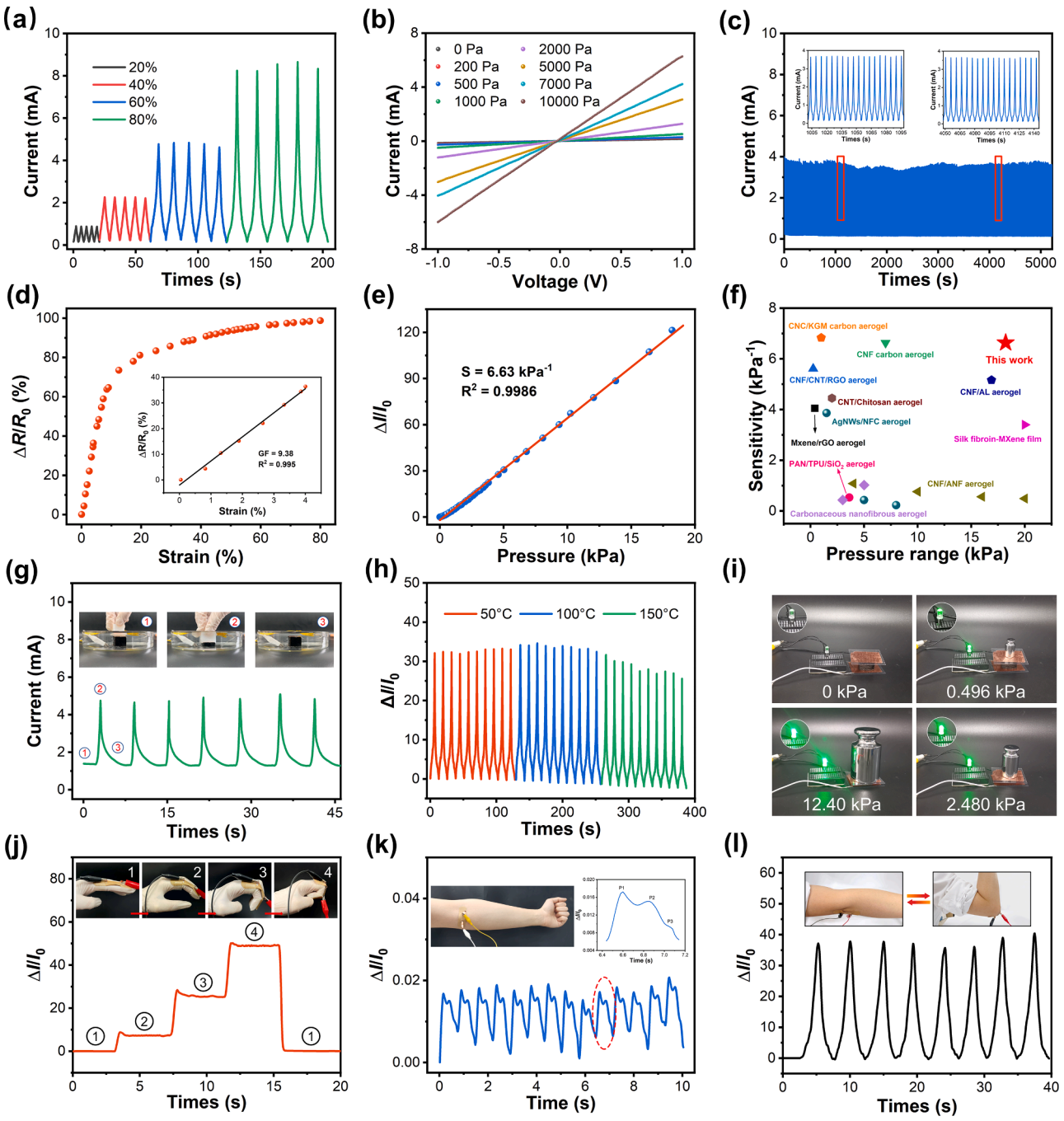

Fig. 5. Pressure-sensing tests and application of a cryogel-based sensor to measure physiological signals. (a) Current response at different strains. (b) *I-V* curves with a voltage ranging from −1 to 1 V at different external pressures. (c) Current stability at 50% strain for 1000 cycles. (d) $\Delta R/R_0$ at 80% strain. (e) Linear sensitivity (*S*) with a working pressure range of 0–18.21 kPa. (f) Comparison of sensitivity *versus* working pressure range of PPy@CNF/SiO_2 compared to other reported sensing materials [43–53]. (g) Current response through underwater compression. (h) Multiple-cycle sensing performance of PPy@CNF/SiO_2 cryogel in high temperature environment. (i) LED brightness changes under different pressures. Detection of (j) finger bending at various angles, (k) arm pulse and (l) elbow bending.

in regular blood pulse signals (periodicity of about 81 beats min^{-1}, Fig. 5k), including three peaks corresponding to incoming blood wave (*P*1), ejected by left ventricular wave (*P*2), and reflected wave (*P*3). This demonstration confirmed that the PPy@CNF/SiO_2 system sensed with high precision, subtle changes in pulse signals. The PPy@CNF/SiO_2-based sensor also enabled rapid sensing of large bending motions (elbow), accurately recording the current signals (Fig. 5l). The repeatable $\Delta I/I_0$ signal was highly reversible and stable during multiple bending/relaxing cycles, indicating suitability to monitor dynamic motion.

4. Conclusions

In summary, we demonstrated a simple strategy to synthesize CNF-based dual nanofiber cryogels comprising a cellular structure formed *via* ice crystals, which displayed superelasticity, thermal insulation and electroactive properties. CNF formed a 3D-network intertwined with flexible SiO_2 nanofibers, resulting in a highly-ordered porous structure. The cellular structure not only effectively dissipated stress, but also contributed to good thermal insulation (29.65 mW m^{-1} K^{-1}). Given the excellent mechanical strength and flexibility, as well as unique internal porous architecture, the CNF/SiO_2 cryogels were modified with

conductive PPy to develop electroactive (sensing) devices. The PPy@CNF/SiO_2-based sensor showed excellent sensitivity (up to 6.63 kPa^{-1}) and detected a broad range of pressures (0–18 kPa) with an excellent durability (1000 cycles). The presented hybrid materials represent a facile, low-cost, and scalable approach based on nanocellulose cryogels that achieve a superior performance inspired by natural, cellular materials. The introduced dual nanofiber cryogels offer a pathway to create high-performance, multifunctional and superelastic platforms that compete or outperform carbon-based materials for the next-generation wearable electroactive materials, particularly for applications under various environments.

Declaration of Competing Interest

The authors declare that they have no known competing financial interests or personal relationships that could have appeared to influence the work reported in this paper.

Data availability

Data will be made available on request.

Acknowledgements

This work was supported by the Innovation Foundation for Doctoral Program of Forestry Engineering of Northeast Forestry University (LYGC202106), the Natural Science Foundation of Heilongjiang Province (LH2020C039, YQ2021C008 and YQ2021C009), and the China Postdoctoral Science Foundation (2021M700734). O.J.R. and L.B. also acknowledge funding support from the Canada Excellence Research Chair Program (CERC-2018-00006), the Canada Foundation for Innovation (Project number 38623), and the European Research Council under the European Union's Horizon 2020 research and innovation program (ERC Advanced grant No. 788489, "BioElCell").

Appendix A. Supplementary data

Supplementary data to this article can be found online at https://doi.org/10.1016/j.cej.2022.140638.

References

[1] W. Jiang, C. Yao, W. Chen, D. Li, L. Zhong, C. Liu, A super-resilient and highly sensitive graphene oxide/cellulose-derived carbon aerogel, J. Mater. Chem. A 8 (35) (2020) 18376–18384.
[2] K. Wu, L. Zhang, Y. Yuan, L. Zhong, Z. Chen, X. Chi, H. Lu, Z. Chen, R. Zou, T. Li, C. Jiang, Y. Chen, X. Peng, J. Lu, An iron-decorated carbon aerogel for rechargeable flow and flexible Zn-air batteries, Adv. Mater. 32 (32) (2020) e2002292.
[3] S. Han, N.U.H. Alvi, L. Granlof, H. Granberg, M. Berggren, S. Fabiano, X. Crispin, A multiparameter pressure-temperature-humidity sensor based on mixed ionic-electronic cellulose aerogels, Adv. Sci. 6 (8) (2019) 1802128.
[4] H. Liu, X. Chen, Y. Zheng, D. Zhang, Y. Zhao, C. Wang, C. Pan, C. Liu, C. Shen, Lightweight, superelastic, and hydrophobic polyimide nanofiber /MXene composite aerogel for wearable piezoresistive sensor and oil/water separation applications, Adv. Funct. Mater. 31 (13) (2021) 2008006.
[5] D. Jiang, J. Zhang, S. Qin, Z. Wang, K.A.S. Usman, D. Hegh, J. Liu, W. Lei, J. M. Razal, Superelastic Ti3C2Tx MXene-based hybrid aerogels for compression-resilient devices, ACS Nano 15 (3) (2021) 5000–5010.
[6] J. Wang, D. Liu, Q. Li, C. Chen, Z. Chen, P. Song, J. Hao, Y. Li, S. Fakhrhoseini, M. Naebe, X. Wang, W. Lei, Lightweight, superelastic yet thermoconductive boron nitride nanocomposite aerogel for thermal energy regulation, ACS Nano 13 (7) (2019) 7860–7870.
[7] T. Su, N. Liu, D. Lei, L. Wang, Z. Ren, Q. Zhang, J. Su, Z. Zhang, Y. Gao, Flexible MXene/bacterial cellulose film sound detector based on piezoresistive sensing mechanism, ACS Nano 16 (2022) 8461–8471.
[8] Y. Huang, X. Fan, S.C. Chen, N. Zhao, Emerging technologies of flexible pressure sensors: Materials, modeling, devices, and manufacturing, Adv. Funct. Mater. 29 (12) (2019) 1808509.
[9] F. Wang, L. Dou, J. Dai, Y. Li, L. Huang, Y. Si, J. Yu, B. Ding, In situ synthesis of biomimetic silica nanofibrous aerogels with temperature-invariant superelasticity over one million compressions, Angew. Chem. Int. Ed. 59 (21) (2020) 8285–8292.
[10] L. Dou, X. Zhang, X. Cheng, Z. Ma, X. Wang, Y. Si, J. Yu, B. Ding, Hierarchical cellular structured ceramic nanofibrous aerogels with temperature-invariant superelasticity for thermal insulation, ACS Appl. Mater. Interfaces 11 (32) (2019) 29056–29064.
[11] Z.L. Yu, B. Qin, Z.Y. Ma, J. Huang, S.C. Li, H.Y. Zhao, H. Li, Y.B. Zhu, H.A. Wu, S. H. Yu, Superelastic hard carbon nanofiber aerogels, Adv. Mater. 31 (23) (2019) e1900651.
[12] X. Gui, J. Wei, K. Wang, A. Cao, H. Zhu, Y. Jia, Q. Shu, D. Wu, Carbon nanotube sponges, Adv. Mater. 22 (5) (2010) 617–621.
[13] P. Song, B. Liu, C. Liang, K. Ruan, H. Qiu, Z. Ma, Y. Guo, J. Gu, Lightweight, flexible cellulose-derived carbon aerogel@reduced craphene oxide/PDMS composites with outstanding EMI shielding performances and excellent thermal conductivities, Nano-Micro Lett. 13 (1) (2021) 91.
[14] C. Cai, Z. Wei, Y. Huang, Y. Fu, Wood-inspired superelastic MXene aerogels with superior photothermal conversion and durable superhydrophobicity for clean-up of super-viscous crude oil, Chem. Eng. J. 421 (2021), 127772.
[15] Z. Qin, Y. Lv, X. Fang, B. Zhao, F. Niu, L. Min, K. Pan, Ultralight polypyrrole crosslinked nanofiber aerogel for highly sensitive piezoresistive sensor, Chem. Eng. J. 427 (2022), 131650.
[16] V. Rahmanian, T. Pirzada, S. Wang, S.A. Khan, Cellulose-based hybrid aerogels: Strategies toward design and functionality, Adv. Mater. 33 (51) (2021) e2102892.
[17] L. Dou, Y. Si, J. Yu, B. Ding, Semi-template based, biomimetic-architectured, and mechanically robust ceramic nanofibrous aerogels for thermal insulation, Nano Res. 15 (6) (2022) 5581–5589.
[18] H.-Y. Mi, H. Li, X. Jing, Q. Zhang, P.-Y. Feng, P. He, Y. Liu, Superhydrophobic cellulose nanofibril/silica fiber/Fe3O4 nanocomposite aerogel for magnetically driven selective oil absorption, Cellul. 27 (15) (2020) 8909–8922.
[19] H.-J. Zhan, K.-J. Wu, Y.-L. Hu, J.-W. Liu, H. Li, X. Guo, J. Xu, Y. Yang, Z.-L. Yu, H.-L. Gao, X.-S. Luo, J.-F. Chen, Y. Ni, S.-H. Yu, Biomimetic carbon tube aerogel enables super-elasticity and thermal insulation, Chem 5 (7) (2019) 1871–1882.
[20] X. Dong, W. Gan, Y. Shang, J. Tang, Y. Wang, Z. Cao, Y. Xie, J. Liu, L. Bai, J. Li, O. J. Rojas, Low-value wood for sustainable high-performance structural materials, Nat. Sustain. 5 (2022) 628–635.
[21] W. Chen, H. Yu, S.Y. Lee, T. Wei, J. Li, Z. Fan, Nanocellulose: A promising nanomaterial for advanced electrochemical energy storage, Chem. Soc. Rev. 47 (8) (2018) 2837–2872.
[22] C. Chen, L. Hu, Nanoscale ion regulation in wood-based structures and their device applications, Adv. Mater. 33 (28) (2021) e2002890.
[23] J. Song, C. Chen, Z. Yang, Y. Kuang, T. Li, Y. Li, H. Huang, I. Kierzewski, B. Liu, S. He, T. Gao, S.U. Yuruker, A. Gong, B. Yang, L. Hu, Highly compressible, anisotropic aerogel with aligned cellulose nanofibers, ACS Nano 12 (1) (2018) 140–147.
[24] C. Chen, J. Song, S. Zhu, Y. Li, Y. Kuang, J. Wan, D. Kirsch, L. Xu, Y. Wang, T. Gao, Y. Wang, H. Huang, W. Gan, A. Gong, T. Li, J. Xie, L. Hu, Scalable and sustainable approach toward highly compressible, anisotropic, lamellar carbon sponge, Chem 4 (3) (2018) 544–554.
[25] H. Guan, Z. Cheng, X. Wang, Highly compressible wood sponges with a spring-like lamellar structure as effective and reusable oil absorbents, ACS Nano 12 (10) (2018) 10365–10373.
[26] Z.Z. Pan, H. Nishihara, S. Iwamura, T. Sekiguchi, A. Sato, A. Isogai, F. Kang, T. Kyotani, Q.H. Yang, Cellulose nanofiber as a distinct structure-directing agent for xylem-like microhoneycomb monoliths by unidirectional freeze-drying, ACS Nano 10 (12) (2016) 10689–10697.
[27] T. Huang, Y. Zhu, J. Zhu, H. Yu, Q. Zhang, M. Zhu, Self-reinforcement of light, temperature-resistant silica nanofibrous aerogels with tunable mechanical properties, Adv. Fiber Mater. 2 (6) (2020) 338–347.
[28] Z. Qin, S. Zhao, X. Fang, B. Zhao, J. Deng, K. Pan, Flexible, ultra-light, and 3D designed white-light-emitting nanofiber aerogel, Adv. Funct. Mater. 32 (6) (2022) 2109240.
[29] Z. Zhang, G. Sèbe, D. Rentsch, T. Zimmermann, P. Tingaut, Ultralightweight and flexible silylated nanocellulose sponges for the selective removal of oil from water, Chem. Mater. 26 (8) (2014) 2659–2668.
[30] N. Lavoine, L. Bergström, Nanocellulose-based foams and aerogels: processing, properties, and applications, J. Mater. Chem. A 5 (31) (2017) 16105–16117.
[31] M. Dilamian, M. Joghataei, Z. Ashrafi, C. Bohr, S. Mathur, H. Maleki, From 1D electrospun nanofibers to advanced multifunctional fibrous 3D aerogels, Appl. Mater. Today 22 (2021), 100964.
[32] Y. Wang, L. Chen, H. Cheng, B. Wang, X. Feng, Z. Mao, X. Sui, Mechanically flexible, waterproof, breathable cellulose/polypyrrole/polyurethane composite aerogels as wearable heaters for personal thermal management, Chem. Eng. J. 402 (2020), 126222.
[33] X. Dong, Y. Si, C. Chen, B. Ding, H. Deng, Reed leaves inspired silica nanofibrous aerogels with parallel-arranged vessels for salt-resistant solar desalination, ACS Nano 15 (2021) 12256–12266.
[34] S. Jiang, M. Zhang, W. Jiang, Q. Xu, J. Yu, L. Liu, L. Liu, Multiscale nanocelluloses hybrid aerogels for thermal insulation: The study on mechanical and thermal properties, Carbohydr. Polym. 247 (2020), 116701.
[35] S. Jiang, M. Zhang, M. Li, L. Liu, L. Liu, J. Yu, Cellulose nanofibril (CNF) based aerogels prepared by a facile process and the investigation of thermal insulation performance, Cellul. 27 (11) (2020) 6217–6233.
[36] M. Yan, Y. Pan, X. Cheng, Z. Zhang, Y. Deng, Z. Lun, L. Gong, M. Gao, H. Zhang, "Robust-soft" anisotropic nanofibrillated cellulose aerogels with superior mechanical, flame-retardant, and thermal insulating properties, ACS Appl. Mater. Interfaces 13 (23) (2021) 27458–27470.
[37] A. Lendlein, O.E.C. Gould, Reprogrammable recovery and actuation behaviour of shape-memory polymers, Nat. Rev. Mater. 4 (2) (2019) 116–133.

[38] Q. Fu, Y. Si, C. Duan, Z. Yan, L. Liu, J. Yu, B. Ding, Highly carboxylated, cellular structured, and underwater superelastic nanofibrous aerogels for efficient protein separation, Adv. Funct. Mater. 29 (13) (2019) 1808234.
[39] J. Zhang, Y. Cheng, M. Tebyetekerwa, S. Meng, M. Zhu, Y. Lu, "Stiff-soft" binary synergistic aerogels with superflexibility and high thermal insulation performance, Adv. Funct. Mater. 29 (15) (2019) 1806407.
[40] X. Zhang, X. Zhao, T. Xue, F. Yang, W. Fan, T. Liu, Bidirectional anisotropic polyimide/bacterial cellulose aerogels by freeze-drying for super-thermal insulation, Chem. Eng. J. 385 (2020), 123963.
[41] B. Wicklein, A. Kocjan, G. Salazar-Alvarez, F. Carosio, G. Camino, M. Antonietti, L. Bergstrom, Thermally insulating and fire-retardant lightweight anisotropic foams based on nanocellulose and graphene oxide, Nat. Nanotechnol. 10 (3) (2015) 277–283.
[42] Y. Ma, N. Liu, L. Li, X. Hu, Z. Zou, J. Wang, S. Luo, Y. Gao, A highly flexible and sensitive piezoresistive sensor based on MXene with greatly changed interlayer distances, Nat. Commun. 8 (1) (2017) 1207.
[43] Z. Chen, H. Zhuo, Y. Hu, H. Lai, L. Liu, L. Zhong, X. Peng, Wood-derived lightweight and elastic carbon aerogel for pressure sensing and energy storage, Adv. Funct. Mater. 30 (17) (2020) 1910292.
[44] S. Wang, W. Meng, H. Lv, Z. Wang, J. Pu, Thermal insulating, light-weight and conductive cellulose/aramid nanofibers composite aerogel for pressure sensing, Carbohydr. Polym. 270 (2021), 118414.
[45] H. Zhuo, Y. Hu, Z. Chen, X. Peng, H. Lai, L. Liu, Q. Liu, C. Liu, L. Zhong, Linking renewable cellulose nanocrystal into lightweight and highly elastic carbon aerogel, ACS Sustain. Chem. Eng. 8 (32) (2020) 11921–11929.
[46] H. Liu, T. Xu, C. Cai, K. Liu, W. Liu, M. Zhang, H. Du, C. Si, K. Zhang, Multifunctional superelastic, superhydrophilic, and ultralight nanocellulose-based composite carbon aerogels for compressive supercapacitor and strain sensor, Adv. Funct. Mater. 32 (26) (2022) 2113082.
[47] H. Lai, H. Zhuo, Y. Hu, G. Shi, Z. Chen, L. Zhong, M. Zhang, Anisotropic carbon aerogel from cellulose nanofibers featuring highly effective compression stress transfer and pressure sensing, ACS Sustain. Chem. Eng. 9 (29) (2021) 9761–9769.
[48] Y. Si, X. Wang, C. Yan, L. Yang, J. Yu, B. Ding, Ultralight biomass-derived carbonaceous nanofibrous aerogels with superelasticity and high pressure-sensitivity, Adv. Mater. 28 (43) (2016) 9512–9518.
[49] D. Wang, L. Wang, Z. Lou, Y. Zheng, K. Wang, L. Zhao, W. Han, K. Jiang, G. Shen, Biomimetic, biocompatible and robust silk Fibroin-MXene film with stable 3D cross-link structure for flexible pressure sensors, Nano Energy 78 (2020), 105252.
[50] Z. Ouyang, C. Wang, D. Xu, H.Y. Yu, Y. Zhou, M. Mu, D. Ge, Z. Miao, K.C. Tam, Lightweight nanofibrous crosslinked composite aerogels with controllable shapes and superelasticity for pressure sensors, Macromol. Mater. Eng. 307 (2022) 2100834.
[51] R. Cheng, J. Zeng, B. Wang, J. Li, Z. Cheng, J. Xu, W. Gao, K. Chen, Ultralight, flexible and conductive silver nanowire/nanofibrillated cellulose aerogel for multifunctional strain sensor, Chem. Eng. J. 424 (2021) 13051565.
[52] Y. Ma, Y. Yue, H. Zhang, F. Cheng, W. Zhao, J. Rao, S. Luo, J. Wang, X. Jiang, Z. Liu, N. Liu, Y. Gao, 3D synergistical MXene/reduced graphene oxide aerogel for a piezoresistive sensor, ACS Nano 12 (4) (2018) 3209–3216.
[53] Q. Luo, H. Zheng, Y. Hu, H. Zhuo, Z. Chen, X. Peng, L. Zhong, Carbon nanotube/chitosan-based elastic carbon aerogel for pressure sensing, Ind. Eng. Chem. Res. 58 (38) (2019) 17768–17775.